Model Based Design of Balancing Systems for Electric Vehicle Battery Packs

Thomas Bruen*, James Marco*
Miguel Gama**

** WMG, University of Warwick, Coventry, United Kingdom (e-mail: thomas.bruen@warwick.ac.uk)*
***Jaguar Land Rover, Coventry, United Kingdom*

Abstract: Battery packs containing multiple cells in series require a balancing system in order to ensure energy and power requirements for the battery pack are maintained throughout its life. Based on the equivalent circuit model (ECM) of a cell, a new framework is proposed which can accommodate a control-oriented model of a balancing system while maintaining the same measured input and output as an ECM. This allows for model-based design of the balancing control system and other battery management system functions such as state estimation. Three examples of balancing system models are presented to show how balancing systems can be designed and analyzed. A model-based controller is then designed for one balancing system to show how the framework can be used to generate less heat while removing imbalance at the same rate.

Keywords: Energy Management; Batteries; Control Design.

1. INTRODUCTION

Cell models are often used as part of the battery management system (BMS) for an electric vehicle (EV), for functions such as estimating state of charge (SOC) and available power. Commonly an equivalent circuit model (ECM) is used due to its simplicity and real-time capability, see for example Fleischer et al. (2014). The BMS must control a cell balancing system which charges and/or discharges individual cells in order to reduce differences in cell voltage, SOC or charge, which can negatively impact the power and energy capability of the pack. Such imbalance can occur due to variations in manufacturing, operating temperature and differing rates of cell degradation, see Dubarry et al. (2010). Balancing systems are typically classed as passive or active. Passive systems dissipate excess charge as heat through a resistor, whereas active systems are able to distribute charge between cells. Cell voltage is commonly used as a metric of imbalance due to it being a measured signal rather than an estimate – see Lu et al. (2013). However, as discussed by Young et al. (2013), differences in impedance mean that cells at the same voltage can be at different SOCs. An accurate SOC estimation could therefore be considered an improvement on voltage measurement. Capacity differences between cells mean that cells at the same SOC may be storing different amounts of charge, and so could still be considered imbalanced.

Balancing systems affect the response of the cells. The cell current and terminal voltage are changed, which in turn may mislead the BMS about the level of imbalance. Reviews of balancing systems by Baronti et al. (2014) and Gallardo-Lozano et al. (2014) give high level behavioural models. While these may give an indication of charge transferred over the several hour duration of balancing, they have limited accuracy. For example it is assumed the balancing current is constant, and there is no insight into cell response. Similarly, papers on specific balancing systems such as by Lin et al. (2011) and Lee & Cheng (2005) provide equations for balancing current but do not couple this with the control system or cell model. Algorithms for controlling the balancing system are also not model based and are often open loop, typically based on periodically checking the cells' voltages and switching cell balancing circuits on or off accordingly, see for example Lee et al. (2011), Zhi-guo et al. (2006). Algorithms for specific balancing systems are proposed in Samadi & Saif (2014) and Altaf et al. (2012), which show the potential for using model predictive control. Both rely on genetic algorithms to solve a nonlinear constrained minimization function, which is computationally expensive for real time applications.

This paper introduces a new methodology for developing ECMs which incorporate balancing systems while maintaining the same inputs and outputs as the standard ECM. These can be used for model-based design and control, in particular designing a regulator rather than relying on open-loop control or very limited feedback. In the first section, the standard ECM is introduced. This is modified to a form suited to the inclusion of balancing systems, and then a generalized solution is proposed. Next, three different balancing topologies are modelled to show how this model structure can be applied, with example simulation results and comments on the implications of the model. Finally the benefits of using the framework for controller design are demonstrated by using it to simulate optimal control of a passive balancing system.

2. CELL MODEL

The ECM is widely reported in literature, with many variants possible, see for example Hu et al. (2012) and He et al. (2011). A schematic of a two state ECM is shown in Figure 1 which for a given cell current i_{cell}, produces a terminal voltage v_t. The circuit consists of an open-circuit voltage v_{OC}, direct resistance R_D and resistor-capacitor (RC) pair R_p and C_p. For brevity only

one RC pair has been used to capture polarisation voltage, though several with different time constants can be used to increase bandwidth and model accuracy. The governing equations for v_t, v_p, SOC and v_{OC} are given by (1)-(4) respectively. In (3), Q is the cell capacity in Ah, and 36 is a factor used to rescale the charge value to a percentage.

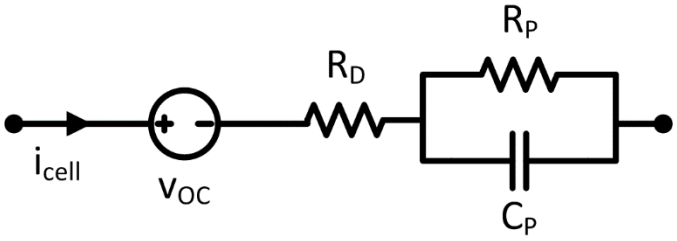

Figure 1: Schematic of equivalent circuit model

$$v_t = v_{OC} + v_p + R_D i_{cell} \tag{1}$$

$$\dot{v_p} = -\frac{v_p}{R_p C_p} + \frac{i_{cell}}{C_p} \tag{2}$$

$$\dot{SOC} = \frac{i_{cell}}{36Q} \tag{3}$$

$$v_{oc} = f(SOC) \tag{4}$$

Typically, SOC is used as a state, but here v_{OC} is used instead to facilitate matrix manipulation of balancing models. The state equation is given by (5) and can be seen to be analogous to (3). For an ECM, a one-to-one relationship between SOC and v_{OC} is assumed and so the states are interchangeable. An effective capacitance, C_0, is calculated using (6) which is analogous to the integrating factor for SOC, and the system poles are the same as for when SOC is a state.

$$\dot{v_{OC}} = \frac{i_{cell}}{C_0} \tag{5}$$

$$C_0(v_{OC}) = 36Q\frac{dSOC(v_{OC})}{dv_{OC}} \tag{6}$$

The model parameters are typically a function of SOC/v_{OC} and temperature, but for simplicity a linearized case is considered here. In linear state-space form (7), the system is written as (8). Note also that by using v_{OC} as a state, the nonlinear function (4) is now captured by a parameter, C_0. The output equation is now linear parameter varying rather than nonlinear, while the state equations are maintained as linear parameter varying. This potentially simplifies controller design.

$$\begin{aligned} \dot{\boldsymbol{x}} &= A\boldsymbol{x} + B\boldsymbol{u} \\ \boldsymbol{y} &= C\boldsymbol{x} + D\boldsymbol{u} \end{aligned} \tag{7}$$

$$\begin{bmatrix} \dot{v_{oc}} \\ \dot{v_p} \end{bmatrix} = \begin{bmatrix} 0 & 0 \\ 0 & -\frac{1}{R_p C_p} \end{bmatrix} \begin{bmatrix} v_{oc} \\ v_p \end{bmatrix} + \begin{bmatrix} \frac{1}{C_0} \\ \frac{1}{C_p} \end{bmatrix} i_{cell} \tag{8}$$

$$[v_t] = [1 \quad 1] \begin{bmatrix} v_{oc} \\ v_p \end{bmatrix} + [R_D] i_{cell}$$

When there is no balancing current, i_{cell} is equal to the applied current i_{app}. For many balancing systems, the balancing current is a function of cell voltage, and possibly the voltages of other cells. As such, the cell current is no longer just the applied current, it also becomes a function of the cell(s)' states. While i_{app} is measured, individual cell currents are typically not due to the cost and complexity of the additional instrumentation, so they cannot form the input to the system model. A generalized equation for i_{cell} is introduced in (9), which is written in a form whereby the model input is i_{app}, while also being a function of the states of that cell. This is achieved by introducing a state dependency matrix E and an input dependency vector F.

$$i_{cell} = E\boldsymbol{x} + F i_{app} \tag{9}$$

An augmented plant model (10) is created by substituting (9) into (8). This means a cell model which incorporates balancing is now feasible, while the input (i_{app}) and output (v_t) are the same as for a conventional cell model, making it suitable for the same real-time applications. Note that if E is a matrix of zeros and F equal to one, the system returns to the non-balancing case.

$$\begin{aligned} \dot{\boldsymbol{x}} &= A'\boldsymbol{x} + B' i_{app} \\ \boldsymbol{y} &= C'\boldsymbol{x} + D' i_{app} \end{aligned}$$

Where:

$$\begin{aligned} A' &= A + BE \\ B' &= BF \\ C' &= C + DE \\ D' &= DF \end{aligned} \tag{10}$$

Several cells can be combined into one state-space framework, by creating block diagonals of each individual matrix and vectorizing the states, input and outputs. These matrices and vectors will be denoted by the superscript M; examples for the A^M matrix and i_{cell}^M vector for N cells are shown in (11), where the subscript index is the cell number. Using the A^M-D^M matrices does not change the dynamics of each cell by itself, but the E^M and F^M matrices can then be populated such that one cell's states can be influenced by another's. The E^M matrix is size NxSN, where N is the number of cells and S the number of states per cell (2 throughout this paper). F^M is an $Nx1$ vector. Generally, the E^M coefficients for each state of a particular cell are the same. As such, it is more convenient to first create an NxN square matrix of coefficients for each cell, then pattern the columns S times using the Kronecker tensor product $\otimes$.

$$A^M = \begin{bmatrix} 0 & \cdots & \cdots & \cdots & \cdots & 0 \\ \vdots & -\frac{1}{R_{p\,1}C_{p\,1}} & & & & \vdots \\ \vdots & & \ddots & & & \vdots \\ \vdots & & & \ddots & & \vdots \\ \vdots & & & & 0 & \vdots \\ 0 & \cdots & \cdots & \cdots & \cdots & -\frac{1}{R_{p\,N}C_{p\,N}} \end{bmatrix} \quad (11)$$

$$\boldsymbol{i}_{cell}^M = \begin{bmatrix} i_{cell\,1} \\ i_{cell\,2} \\ \vdots \\ i_{cell\,N} \end{bmatrix}$$

3. BALANCING MODELS

The system structure in (10) is demonstrated with three examples. For the analysis, cell parameters have been obtained from a 20Ah lithium iron phosphate cell model linearized at 70% SOC. A module consisting of four identical cells in series is simulated, with the parameter values and initial *SOC* of each cell given in Table 1. The applied current was set to zero and the systems set to balance until the cell *SOC*s were within 1% of each other.

Table 1: Model Parameters

Parameter	Value
C_0	226.7kF
R_D	1.75mΩ
R_p	1.02mΩ
C_p	14.0kF
$SOC(0)$	$[73\%\quad 71.5\%\quad 69\%\quad 72\%]^T$

3.1 Passive Balancing

A passive balancing system works by connecting a resistor in parallel with the cell- see for example Lee et al. (2011). This is the most commonly used system on production vehicles due to its low cost and simplicity. However, its dissipative nature means that cell energy is wasted as heat, and energy cannot be distributed between cells. A schematic is shown in Figure 2, where i_{bal} is the balancing current and R_{bal} the balancing resistor. Current is drawn from the cell by the resistor, discharging the cell, with the energy dissipated as heat. The passive system is governed by (12) and (13).

$$i_{cell} = i_{app} - i_{bal} \quad (12)$$

$$v_t = R_{bal} i_{bal} \quad (13)$$

By applying (12) to (1) and substituting this into (13) and rearranging, (14) is obtained. This can be written in the generalized form of (9), where the state dependency matrix and input dependency vector for one cell are given in (15). Since there is no cell interdependence, each cell model can be solved individually.

$$i_{cell} = \frac{-v_{OC} - v_p + R_{bal} i_{app}}{R_D + R_{bal}} \quad (14)$$

$$E = \left[-\frac{1}{R_D + R_{bal}} \quad -\frac{1}{R_D + R_{bal}} \right]$$

$$F = \left[\frac{R_{bal}}{R_D + R_{bal}} \right] \quad (15)$$

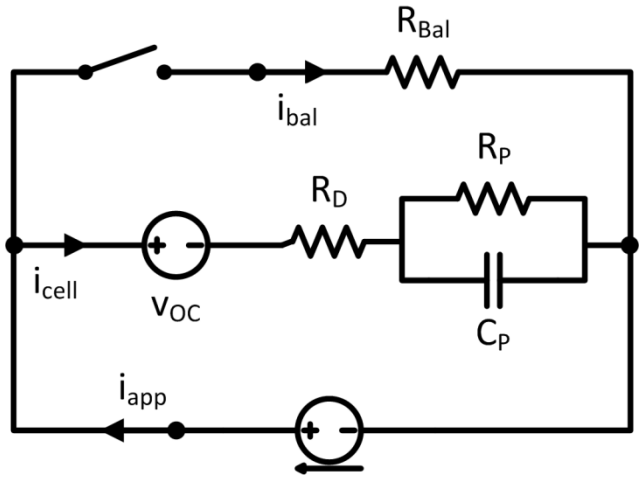

Figure 2: schematic of passive balancing

Figure 3 shows a simulation of passive balancing using a resistance of 8.5Ω which for this model results in a balancing current of approximately 1/50th of the cell capacity. The algorithm used is to activate balancing for all cells which have an *SOC* 1% greater than the minimum *SOC*. The results show a near linear change in *SOC* over time as the balancing current is almost constant. The terminal voltage is pulled down by the balancing current but since the current is small the terminal voltages remain distinct and so are still suitable as a metric of imbalance.

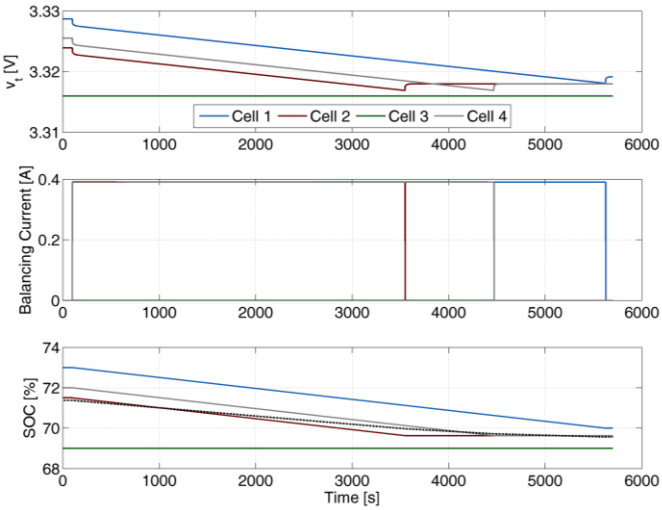

Figure 3: Passive balancing voltage, current and SOC results

3.2 Cell-Cell Capacitive Balancing

A cell-cell capacitive system, a schematic of which is shown in Figure 4, functions by switching a capacitor between two

neighbouring cells. The cell at the higher voltage charges the capacitor, which is then connected to the lower voltage cell. The capacitor then discharges into this cell, and the process is repeated. Two approaches are possible: using a large capacitor and low switching frequency as per Sheng et al. (2011); Arasaratnam et al. (2014), or a small capacitor with a high switching frequency (kHz range), as per Kim et al. (2014). The latter has been chosen here as it would be more cost-effective for an EV.

The model considers a capacitor C_{bal} connected in parallel with a cell; the resistance R_{bal} encapsulates the equivalent series resistance of the capacitor along with transistor resistance. The balancing current is required in order to calculate the cell current using (12). For a capacitive system, the balancing charge also has to be considered, which relates to the current according to (16). The terminal voltage is given by (17), which adds an extra state to the cell model.

$$\dot{q}_{bal} = i_{bal} \tag{16}$$

$$v_t = \frac{q_{bal}}{C_{bal}} + R_{bal}\dot{q_{bal}} \tag{17}$$

Since a BMS sampling rate is typically in the order of 1Hz, modelling the high frequency switching dynamics are not pertinent, and instead a time averaged solution is sought. Over the sub-millisecond time period of the capacitor being connected to the cell, it is assumed that cell state voltages and applied current do not change. The analytical solution for charge q_{bal} transferred while connected to the cell for time t_{SW} is given by (18), with the initial conditions given by (19). The subscripts A and B refer to the cell which is currently connected to the capacitor and the cell which was previously connected respectively.

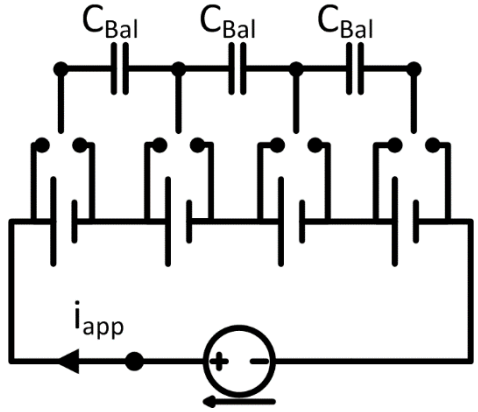

Figure 4: Schematic of cell-cell capacitive system

$$q_{bal\,A}(t_{SW}) = q_{bal\,A}(0)d_A + C_{bal}(1-d_A)(v_{OC\,A} + v_{p\,A} + R_{D\,A}i_{app}) \tag{18}$$

Where:

$$d_A = e^{-\frac{t_{SW}}{C_{bal}(R_{D\,A}+R_{bal})}}$$

$$q_A(0) = C_{bal}(v_{t\,B}(0) - R_{bal}\dot{q}_{bal\,B}(0)) \tag{19}$$

The change in charge over t_{SW} can be calculated to give the average balancing current, $\overline{i_{bal\,A}}$. The average balancing current between BMS samples is then scaled by p, which is the duty cycle (how often the cell is connected to the capacitor) which is taken here to be 0.5. This time-averaged balancing current is given by (20).

$$\overline{i_{bal\,A}} = p\alpha_A\left[-v_{OC\,A} - v_{p\,A} - R_{D\,A}i_{app} + v_{OC\,B} + v_{p\,B} + R_{D\,B}i_{app}\right] \tag{20}$$

Where:

$$\alpha_A = C_{bal}(1-d_A)/t_{SW}$$

A switching matrix, δ, is required to determine which cells are connected to which through each capacitor. From this the respective α values can be calculated and the E^M and F^M matrices can be created: examples are given in (21) for a case where the pairs of balancing cells are 1 and 2, and 3 and 4.

$$\delta = \begin{bmatrix} 0 & 1 & & \\ 1 & 0 & 0 & \\ & 0 & 0 & 1 \\ & & 1 & 0 \end{bmatrix}$$

$$E^M = \begin{bmatrix} -\alpha_1 & \alpha_1 & & \\ \alpha_2 & -\alpha_2 & & \\ & & -\alpha_3 & \alpha_3 \\ & & \alpha_4 & -\alpha_4 \end{bmatrix} \otimes [1 \quad 1] \tag{21}$$

$$F^M = \begin{bmatrix} 1+\alpha_1(R_{D\,2} - R_{D\,1}) \\ 1+\alpha_2(R_{D\,1} - R_{D\,2}) \\ 1+\alpha_3(R_{D\,4} - R_{D\,3}) \\ 1+\alpha_4(R_{D\,3} - R_{D\,4}) \end{bmatrix}$$

For this simulation, the switching frequency was set to 50kHz with a balancing capacitance of 1mF and balancing resistance of 5mΩ. For the values in the simulation, the balancing current was small at the end of the switching period, so the second term in (20) was neglected. Example results are presented in Figure 5. The cell SOCs converge gradually over time and the balancing currents decrease as the cell voltages converge. The balancing current is relatively low: one limiting factor is the balancing resistance which is similar to the cell's internal resistance. As such, the difference in SOCs is largely reflected by the terminal voltages. Figure 6 shows a comparison between (18) and (20) over the duration of the capacitor being connected. The significant variation in balancing current means that using a physical measurement for the BMS could be misleading if consecutive samples are taken at different points throughout the switching cycle. The time-averaged solution provides a much more reliable indication of the state of balancing.

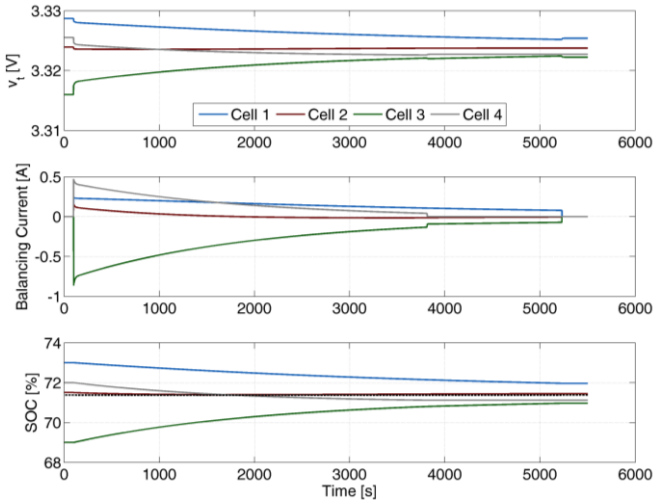

Figure 5: Cell-cell capacitor balancing voltage, current and SOC results

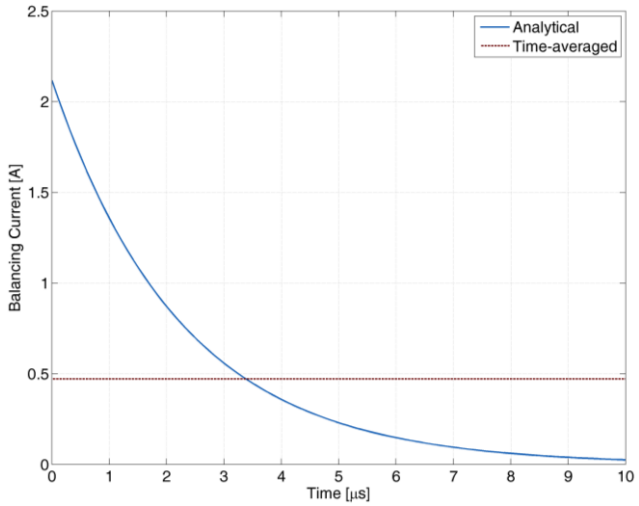

Figure 6: Variation in capacitive balancing current

3.3 Cell-Module Balancing

This balancing system considers the case of a cell discharging into the module or the module charging a cell using a bi-directional converter. A schematic of one cell connected to a module is shown in Figure 7. As discussed in Gallardo-Lozano et al. (2014) and Cao et al. (2008), there are many possible approaches to the hardware design of a cell-module system. For this, the method of voltage conversion is arbitrary, with only the voltage gain g and efficiency η of importance. The equations governing the input and output voltage of the converter are given by (22) and (23), where v_{cell} in this case is the cell connected to the converter input and i_{bal} is the current drawn by the converter input.

$$v_o = g v_{cell} \tag{22}$$

$$i_o = \frac{i_{bal}}{g}\eta \tag{23}$$

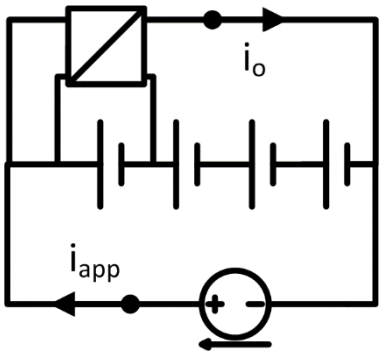

Figure 7: Schematic of cell-to-module balancing system

Additionally, a switching vector, δ, is defined in (24). For the system considered here, only one cell can be connected to the converter at any time. Using this, the vector of cell currents can be written as (25).

$$\delta = \begin{cases} 1, & balancing\ on \\ 0, & balancing\ off \end{cases} \tag{24}$$

$$i_{cell}^{M} = \begin{bmatrix} i_{app} + \dfrac{i_o}{\eta}(\eta - g\delta_1) \\ \vdots \\ i_{app} + \dfrac{i_o}{\eta}(\eta - g\delta_n) \end{bmatrix} \tag{25}$$

When a cell is connected to the module, the converter output is equal to the module voltage and so (26) applies. This can be rearranged to obtain an expression for the converter output current in (27) which can be substituted into (25).

$$g\sum_{n=1}^{N}\delta_n v_{t\,n} = \sum_{n=1}^{N} v_{t\,n} \tag{26}$$

$$i_o = \frac{\sum_{n=1}^{N}(g\delta_n - 1)\left[v_{OC\,n} + v_{p\,n} + R_{D\,n} i_{app}\right]}{\sum_{n=1}^{N}\left[\dfrac{R_{D\,n}}{\eta}(\eta - g\delta_n)(1 - g\delta_n)\right]} \tag{27}$$

From this the E^M and F^M matrices can be derived, which take the form of (28).

$$E^M = \left[\frac{\alpha(\eta - g\delta_n)}{\eta}\,(g\delta_n - 1)^T\right] \otimes [1 \quad 1]$$

$$F^M = \begin{bmatrix} 1 \\ \vdots \\ 1 \end{bmatrix}\left(1 + \alpha\sum_{n=A}^{N} R_0^n\,(G\delta^n - 1)\right) \tag{28}$$

Where:

$$\alpha = \frac{1}{\sum_{n=1}^{N} R_{D\,n}\left[1 + \left(\dfrac{g-\eta}{\eta}\right)\delta_n\right]}$$

For the study considered here, a simple switching algorithm was created which activates balancing for whichever cell is furthest from the mean SOC. The converter gain was set at 4, i.e. the number of cells, and the efficiency at 0.85. Example results are shown in Figure 8.

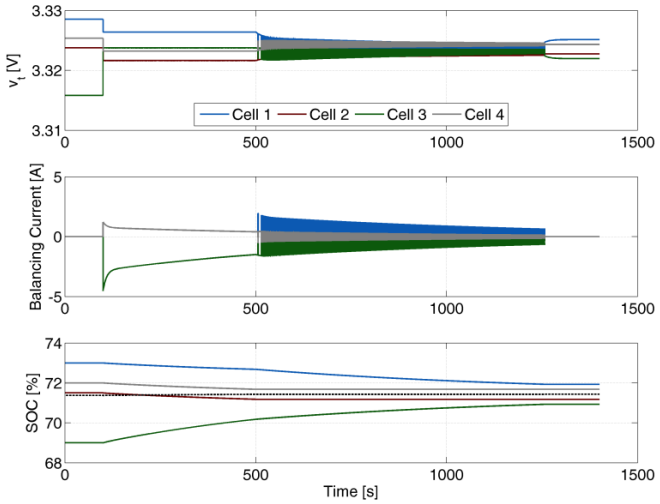

Figure 8: Cell-module converter balancing voltage, current and SOC results

It is apparent that the terminal voltage is changed significantly by the balancing system. For example, once balancing starts, cell 3 has the second highest terminal voltage despite having the lowest SOC. This is because of the large current drawn to charge the cell. As with the cell-cell balancing system, the balancing current reduces over time because it is the difference in cell voltages that drives current magnitude. The cell connected to the converter switches between cell 1 and cell 3 each time step due to each one alternately being further from the mean SOC because the balancing current continually alters the SOC more for the connected cell. The switching signal is shown in Figure 10.

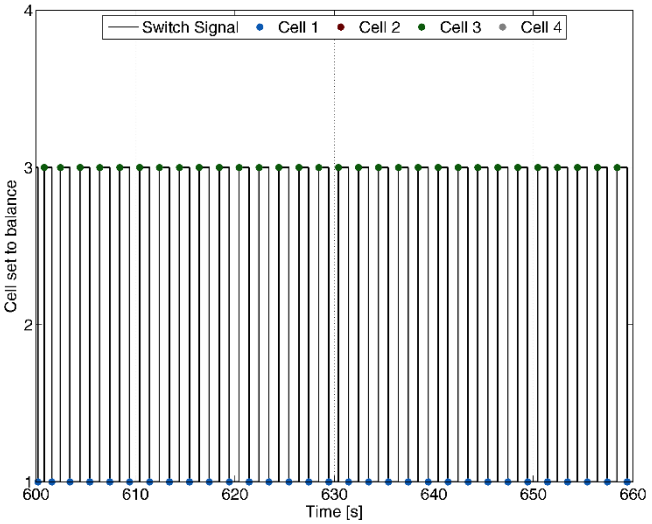

Figure 9: Switching signal over 1 minute period for converter balancing

4. ANALYSIS

Based on the simulation parameters above, the poles of the cell when not balancing and when set to balance are given in Table 2. In all cases, the RC pair poles become faster and the v_{OC} poles are moved from zero to slow, negative values. The passive system has little effect on system poles, due to the relatively large balancing resistance. The current for passive balancing cannot be large due to the amount of heat generated. The converter system creates a larger change in poles than the capacitive system, which is reflected in the faster time to balance.

Table 2: Cell poles for different balancing systems

	No Balancing	Passive	Capacitive	Converter
RC pair pole	-0.07034	-0.07035	-0.07543	-0.11209
v_{OC} pole	0	-5.04E-07	-0.00029	-0.00158

Cell terminal voltage is a commonly used metric of imbalance, see Baughman & Ferdowsi (2005). However, balancing systems alter the terminal voltage, meaning the metric is not necessarily reliable. By using a model of the balancing system, an instantaneous estimate of the terminal voltage without balancing, $\hat{v}_t$, can be made using (29), allowing it to be used as a metric even during balancing. This can also be used to predict and avoid a situation where switching balancing on or off changes the terminal voltage such that it goes outside of the intended region of operation for the cell, which is particularly relevant when balancing toward the end of charging.

$$\hat{v}_t = v_t + R_D i_{bal} \tag{29}$$

If SOC is to be used as an imbalance metric, an accurate SOC estimate is required. Model based approaches such as an extended Kalman Filter are commonly used, see for example Plett (2004) and Sun et al. (2014). These combine cell current integration as per (4) with feedback from the measured cell voltage. Since the balancing system modifies the cell current and voltage, SOC estimation accuracy may be hindered if balancing is not accounted for. In the above examples i_{app} is zero so (4) would yield no change in SOC. The estimator is then dependent on output correction, the rate of which is limited by the robustness of the model. By accounting for balancing in the cell model, better SOC estimation should be possible. Good estimation of balancing current from the model could also mean that balancing current does not need to be sensed, reducing the cost and complexity of the system. Sensing balancing current may not be reliable for some cases anyway, such as for the capacitive system where the current is very dynamic.

5. CONTROLLER DESIGN

The structure of (10) is analogous to a state feedback gain matrix, and the system is controllable according to the rank of the controllability matrix, see Tewari (2002). Techniques such as optimal control could be used to tune the balancing system response, though there may be many constraints on the E^M matrix and F^M vector. The two active systems modelled above lack current control since the balancing current is driven by the state voltages. More control is possible by regulating the converter gain, but the range of gain values must be limited to

avoid taking cell currents and voltages outside the intended operating window. Similarly, the switching frequency of the capacitive system could be altered, with a slower frequency reducing the balancing current. Passive balancing can be regulated by using a duty cycle to alter the time-averaged balancing current. In this case, an effective balancing current $\overline{i_{bal}}$ is calculated using (30) based on a duty cycle d.

$$\overline{i_{bal}} = d\frac{v_t}{R_{bal}} \tag{30}$$

For passive balancing, the cells are to be brought down to within s_d of the lowest SOC in the pack. For this study, s_d was set to be 1%, in line with the examples above. To quantify this, the vector in (31) is created.

$$\Delta SOC = SOC - \min(SOC) - s_d \tag{31}$$

The aim is to find a vector of d values, subject to two criteria. Firstly, all cells should reach end-of-balance simultaneously since some cells finishing earlier than others generates more heat without any additional global imbalance reduction. Secondly, at least one cell should have a duty cycle equal to 1 so the overall imbalance is reduced as fast as possible. In order to meet the first criterion, (32) is used to govern imbalance reduction. By applying (3) and (9), (32) can be written as (33). The objective is to find d for each cell such that (33) applies and at least one d is equal to 1.

$$\Delta SOC \propto \dot{SOC} \tag{32}$$

$$36Q\Delta SOC \propto E^M x + F^M u \tag{33}$$

The state dependency matrix and input dependency vector for cell n are given by (34), derived in the same way as (12)-(15). These can then be diagonalized to create E^M and F^M.

$$E_n = [\alpha_n \quad \alpha_n]$$
$$F_n = \left[\frac{R_{bal}}{R_{D\,n}d_n + R_{bal}}\right] \tag{34}$$

Where:

$$\alpha_n = \frac{d_n}{R_{D\,n}d_n + R_{bal}}$$

The problem can be re-written as (35). Given the relative magnitudes of R_D and R_{bal}, it is assumed that the elements of the input dependency vector are all equal to 1. This is solved by inverting H^M to find a solution to the α^M vector, which is then rescaled such that the maximum d is equal to 1.

$$H^M \alpha^M \propto 36Q\Delta SOC - F^M u$$

Where:

$$H^M = \begin{bmatrix} x_1 + x_2 & & \\ & \ddots & \\ & & x_{end-1} + x_{end} \end{bmatrix} \tag{35}$$

A study with the same initial conditions was run as before, but with a 10% variation in cell internal resistance and capacity. This means that the required duty cycle is no longer just proportional to the SOC difference. Differences in capacity means it will take different amounts of charge to reduce SOC by a given amount, and differences in resistance result in different cell currents for a given duty cycle. The results in Figure 10 show that the three cells all reach the 1% threshold simultaneously, meaning that the minimum possible balancing temperature rise has occurred.

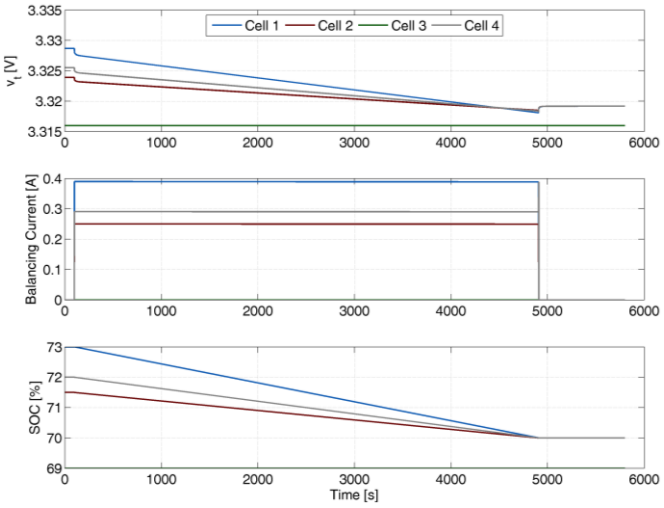

Figure 10: Passive balancing with duty cycle control

If cells 2 and 4 are set to balance with a duty cycle of 1, more power, and so heat is generated, but the global imbalance of the pack is not reduced since this is governed by the difference between cells 1 and 3.

6. CONCLUSIONS

The work presented here provides a standard framework for incorporating a balancing system into a widely used cell model. By directly using v_{OC} as a state, the same inputs and outputs as the standard ECM can be maintained and the same analysis and control techniques applied. This has the benefit of capturing the altered dynamics of the system, so that the variation in cell current and voltage caused by the balancing system can be understood and accounted for, and modelled in real time. Similarly, the impact of which imbalance metric to use (voltage, SOC or charge difference) can also be evaluated. The framework can also be used to design the balancing controller, improving on existing algorithms by accounting for variations in cell properties and incorporating metrics such as time to balance and heat generation.

Future work will include the design of a balancing controller for specific hardware. This also includes accounting for, and analysing the impact of, the parameter varying nature of the system, as well as ensuring robustness to a non-zero applied current.

ACKNOWLEDGMENTS

The research presented within this paper is supported by the Engineering and Physical Science Research Council (EPSRC - EP/ I01585X/1) through the Engineering Doctoral Centre in High Value, Low Environmental Impact Manufacturing. The

research was undertaken in collaboration with the WMG Centre High Value Manufacturing Catapult (funded by Innovate UK) in collaboration with Jaguar Land Rover.

REFERENCES

Altaf, F., Johannesson, L. & Egardt, B. (2012). Evaluating the Potential for Cell Balancing using a Cascaded Multi-Level Converter using Convex Optimization. In *2012 Workshop on Engine and Powertrain Control, Simulation and Modeling*. pp. 100–107.

Arasaratnam, I., Tjong, J. & Habibi, S. (2014). Switched-Capacitor Cell Balancing: A Fresh Perspective.

Baronti, F., Roncella, R. & Saletti, R. (2014). Performance comparison of active balancing techniques for lithium-ion batteries. *Journal of Power Sources*, 267, pp.603–609.

Baughman, A. & Ferdowsi, M. (2005). Battery Charge Equalization-State of the Art and Future Trends. In *Future Transportation Technology Conferencee*. Chicago: SAE International.

Cao, J., Schofield, N. & Emadi, A. (2008). Battery balancing methods: A comprehensive review. In *Vehicle Power and Propulsion Conference, 2008. VPPC '08. IEEE*. pp. 1–6.

Dubarry, M., Vuillaume, N. & Liaw, B.Y. (2010). Origins and accommodation of cell variations in Li-ion battery pack modeling. *International Journal of Energy Research*, 34(2), pp.216–231.

Fleischer, C. et al. (2014). On-line adaptive battery impedance parameter and state estimation considering physical principles in reduced order equivalent circuit battery models. *Journal of Power Sources*, 260, pp.276–291.

Gallardo-Lozano, J. et al. (2014). Battery equalization active methods. *Journal of Power Sources*, 246(0), pp.934–949.

He, H., Xiong, R. & Fan, J. (2011). Evaluation of Lithium-Ion Battery Equivalent Circuit Models for State of Charge Estimation by an Experimental Approach. *Energies*, 4(12), pp.582–598.

Hu, X., Li, S. & Peng, H. (2012). A comparative study of equivalent circuit models for Li-ion batteries. *Journal of Power Sources*, 198, pp.359–367.

Kim, M.-Y. et al. (2014). A Chain Structure of Switched Capacitor for Improved Cell Balancing Speed of Lithium-Ion Batteries. *Industrial Electronics, IEEE Transactions on*, 61(8), pp.3989–3999.

Lee, W.C. et al. (2011). Comparison of passive cell balancing and active cell balancing for automotive batteries. In *Vehicle Power and Propulsion Conference (VPPC), 2011 IEEE*. Ieee, pp. 1–7.

Lee, Y.-S. & Cheng, M.-W. (2005). Intelligent control battery equalization for series connected lithium-ion battery strings. *Industrial Electronics, IEEE Transactions on*, 52(5), pp.1297–1307.

Lin, C. et al. (2011). Battery management system with dual-balancing mechanism for LiFePO<inf>4</inf> battery module. In *TENCON 2011 - 2011 IEEE Region 10 Conference*. Ieee, pp. 863–867.

Lu, L. et al. (2013). A review on the key issues for lithium-ion battery management in electric vehicles. *Journal of Power Sources*, 226(0), pp.272–288.

Plett, G.L. (2004). Extended Kalman filtering for battery management systems of LiPB-based HEV battery packs: Part 1. Background. *Journal of Power Sources*, 134(2), pp.252–261.

Samadi, M.F. & Saif, M. (2014). Nonlinear model predictive control for cell balancing in Li-ion battery packs. *American Control Conference (ACC), 2014*, pp.2924–2929.

Sheng, C. et al. (2011). Implementation of cell balancing with super-capacitor for robot power system. In *Intelligent Control and Automation (WCICA), 2011 9th World Congress on*. Ieee, pp. 468–473.

Sun, F., Xiong, R. & He, H. (2014). Estimation of state-of-charge and state-of-power capability of lithium-ion battery considering varying health conditions. *Journal of Power Sources*, 259, pp.166–176.

Tewari, A. (2002). *Modern Control Design: With MATLAB and SIMULINK*, Wiley.

Young, K. et al. (2013). Electric Vehicle Battery Technologies. In R. Garcia-Valle & J. A. Peças Lopes, eds. *Electric Vehicle Integration into Modern Power Networks*. Springer New York, pp. 15–56.

Zhi-guo, K. et al. (2006). Comparison and Evaluation of Charge Equalization Technique for Series Connected Batteries. *Power Electronics Specialists Conference, 2006. PESC '06. 37th IEEE*, pp.1–6.